Circulation Research
JOURNAL OF THE AMERICAN HEART ASSOCIATION

Imaging Ca^{2+} Nanosparks in Heart with a New Targeted Biosensor

Wei Shang, Fujian Lu, Tao Sun, Jiejia Xu, Lin-Lin Li, Yanru Wang, Gang Wang, Liangyi Chen, Xianhua Wang, Mark B Cannell, Shi-Qiang Wang and Heping Cheng

Circ Res. published online November 20, 2013;
Circulation Research is published by the American Heart Association, 7272 Greenville Avenue, Dallas, TX 75231

Print ISSN: 0009-7330. Online ISSN: 1524-4571

NEW METHODS IN CARDIOVASCULAR BIOLOGY

Imaging Ca^{2+} Nanosparks in Heart with a New Targeted Biosensor

Wei Shang[1], Fujian Lu[1], Tao Sun[1], Jiejia Xu[1], Lin-Lin Li[2] , Yanru Wang[1], Gang Wang[1], Liangyi Chen[1], Xianhua Wang[1], Mark B Cannell[3], Shi-Qiang Wang[2], Heping Cheng[1]

[1]State Key Laboratory of Biomembrane and Membrane Biotechnology, Beijing Key Laboratory of Cardiometabolic Molecular Medicine, Institute of Molecular Medicine, Peking-Tsinghua Center for Life Sciences, Peking University, Beijing 100871, China; [2]State Key Laboratory of Biomembrane and Membrane Biotechnology, College of Life Science, Peking University, Beijing 100871, China, and; [3]Department of Physiology and Pharmacology, Medical Sciences Building, University of Bristol, BS8 1TD U.K.

W.S and F.L. contributed equally to this study.

***Running title*:** Imaging Ca^{2+} Nanosparks in Heart

Subject codes:
[136] Calcium cycling/excitation-contraction coupling
[150] Imaging
[152] Ion channels/membrane transport

Address correspondence to:

Dr. Heping Cheng
Institute of Molecular Medicine
Peking University
Beijing 100871
China
Tel : 86-10-6276-5957
Fax : 86-10-6276-5957
chengp@pku.edu.cn

Dr. Shi-Qiang Wang
College of Life Science
Peking University
Beijing 100871
China
Tel : 86-10-6275-5002
Fax : 86-10-6275-5002
wsq@pku.edu.cn

In October 2013, the average time from submission to first decision for all original research papers submitted to *Circulation Research* was 12.81 days

DOI: 10.1161/CIRCRESAHA.114.302938

ABSTRACT

Rationale: In cardiac dyads, junctional Ca^{2+} directly controls the gating of the ryanodine receptors (RyRs), and is itself dominated by RyR-mediated Ca^{2+} release from the sarcoplasmic reticulum. Existing probes do not report such local Ca^{2+} signals due to probe diffusion, so a junction-targeted Ca^{2+} sensor should reveal new information on cardiac excitation-contraction coupling and its modification in disease *states*.

Objective: To investigate Ca^{2+} signaling in the nanoscopic space of cardiac dyads by targeting a new sensitive Ca^{2+} biosensor (GCaMP6f) to the junctional space.

***Methods and Results*:** By fusing GCaMP6f to the N-terminus of triadin 1 or junctin, GCaMP6f-T/J was targeted to dyadic junctions, where it colocalized with t-tubules and RyRs after adenovirus-mediated gene transfer. This membrane protein-tagged biosensor displayed ~4-times faster kinetics than native GCaMP6f. Confocal imaging revealed junctional Ca^{2+} transients ("Ca^{2+} nanosparks") that were ~50-times smaller in volume than conventional Ca^{2+} sparks (measured with diffusible indicators). The presence of the biosensor did not disrupt normal Ca^{2+} signaling. Because no indicator diffusion occurred, the amplitude and timing of release measurements were improved, despite the small recording volume. We could also visualize co-activation of subclusters of RyRs within a single junctional region, as well as 'quarky' Ca^{2+} release events.

***Conclusions*:** This new, targeted biosensor allows selective visualization and measurement of nanodomain Ca^{2+} dynamics in intact cells and can be used to give mechanistic insights into dyad RyR operation in health as well as in disease states such as when RyRs become orphaned.

Keywords:
Excitation-contraction coupling, ryanodine receptor, triadin, junction, genetically encoded Ca^{2+} Biosensor, calcium sparks

Nonstandard Abbreviations and Acronyms:

RyR	ryanodine receptor
EC coupling	excitation-contraction coupling
CICR	Ca^{2+}-induced Ca^{2+} release
LTCC	L-type Ca^{2+} channel
SR	sarcoplasmic reticulum
GCaMP6f-T	GCaMP6f fused to triadin1
GCaMP6f –J	GCaMP6f fused to junctin
K_{OFF}	dissociation rate constant
K_d	dissociation constant
C	Ca^{2+} concentration
R	normalized fluorescence
nH:	Hill coefficient
F/F_0	normalized fluorescence where F_0 refers to the resting fluorescence
$(F/F_0)_d$	F/F_0 deconvolved with a single-exponential kernel reflecting turn-off rate of the biosensor
F_{min}	minimal fluorescence of the biosensor
F_{max}	maximal fluorescence of the biosensor
τ_{decay}	time constant of the decay of biosensor fluorescence
FDHM	full duration at half maximum
T50	time for 50% decay from peak
FWHM	full width at half maximum

INTRODUCTION

Cardiac contraction is due to intracellular Ca^{2+} release as a result of signaling in a nanoscopic domain, the dyad, formed from the close apposition of the sarcoplasmic reticulum (SR) and surface membranes[1]. Two types of Ca^{2+} channels, the voltage-gated L-type Ca^{2+} channels (LTCCs), which control Ca^{2+} influx elicited by action potentials, and ryanodine receptors (RyRs), which mediate Ca^{2+} release from intracellular stores, reside on the surface and SR membranes of the dyad, respectively. Orthograde LTCC-to-RyR coupling is mediated by the Ca^{2+}-induced Ca^{2+} release (CICR) mechanism while retrograde coupling controls the LTCC current within the same beat[2] .

Whole-cell Ca^{2+} transients during cardiac excitation-contraction (EC) coupling were first seen as aequorin bioluminescence in frog cardiac muscle[3] and in canine Purkinje fibers[4]. The creation of small-molecule chemical fluorescence indicators like fura-2[5] catalyzed an explosion of Ca^{2+} imaging activity in single cardiac myocytes under normal conditions[6] and during Ca^{2+} overload when propagating waves of elevated Ca^{2+} were observed[7]. With the advent of confocal microscopy and the fast, high-contrast Ca^{2+} indicator fluo-3, the discovery of Ca^{2+} sparks[8], which are the result of single-dyad Ca^{2+} signaling, has revolutionized our understanding of cardiac EC coupling and the spatiotemporal summation of $\sim 10^4$ elemental Ca^{2+} sparks results in a global Ca^{2+} transient that controls cell contraction. From the viewpoint of control theory, such "digital" behavior is quintessential for enabling high-speed, high-gain amplification with stability in EC coupling[9, 10]. The process of cardiac EC coupling is therefore a tale of signaling in cellular nanodomains whose regulation remains a focus of intense research worldwide.

However, fluorescent Ca^{2+} imaging techniques with diffusible indicators (e.g. see[11]) do not reveal the underlying Ca^{2+} signaling process nor the behavior of the RyRs at the level of the dyad without considerable computational difficulty and uncertainties (e.g. see[11]). Furthermore, Ca^{2+} sparks are not easily detected once whole-cell release starts and $\sim 10^4$ dyads are activated near synchronously. The measurement of "Ca^{2+} spikes"[12] provided a way to overcome this problem, but it requires the inclusion of high concentrations of an exogenous, slow Ca^{2+} buffer (e.g., EGTA) which will disturb the CICR process as well as other signaling processes that depend on Ca^{2+}. A new method to directly probe dyadic space dynamics could therefore give insightful information into how RyRs are regulated, as well as check the veracity of new models for RyR array operation and release termination[13, 14].

The dyadic space is approximately 10^{-3} fl (1 aL)[15], a volume that would preclude obtaining useful dyadic Ca^{2+} signals using conventional fluorescent probes. Here we describe a new approach to this problem using a targeted high sensitivity biosensor construct for Ca^{2+} -GCaMP6f[16]. By attaching GCaMP6f to the dyad junctional proteins junctin or triadin[17], we show that high signal-to-noise records of Ca^{2+} changes in the dyad, which we call "Ca^{2+} nanosparks", can be obtained without complications from indicator diffusion. Ca^{2+} nanosparks are ~50 times smaller in volume than Ca^{2+} sparks and can display substructure and gradation at the single dyad level. We also present exemplar data from adult rat cardiac myocytes showing evoked Ca^{2+} signals at single dyads which should afford a new way of investigating spatiotemporal synchrony (or dyssychrony) in EC coupling in heath and disease.

METHODS

Adult rat cardiac myocytes isolation, culture, and adenovirus infection.

Animals were treated in compliance with the Guide for the Care and Use of Laboratory animals published by the US National Institutes of Health (NIH Publication No.85-23, revised 1996) and approved by the Institutional Animal Care and Use Committee of Peking University (accredited by AAALAC international). Single ventricular myocytes were enzymatically isolated from the hearts of adult male

Sprague–Dawley rats (200–250 g), as described previously[18]. Freshly isolated cardiac myocytes were plated on culture dishes coated with laminin (Sigma) for 1 hour and then the attached cells were cultured in M199 medium (Sigma) added with (in mmol/L) 5 creatine, 2 L-carnitine, 5 taurine, 25 HEPES (all from Sigma), and insulin-transferrin-selenium-X (Gibco). Cardiac myocytes were then infected with adenovirus carrying the target gene at an m.o.i. of 20 and experiments were performed after 48 hours in culture.

Recombinant adenovirus production.

The GCaMP6f gene was amplified from pGP-CMV-GCaMP6f (Addgene, plasmid 40755) and inserted into pEGFP-C1 (Clontech). The rat triadin 1 and junctin genes were cloned and integrated into pEGFP-C1-GCaMP6f with GCaMP6f at the N terminus. The fusion genes GCaMP6f-triadin 1 and GCaMP6f-junctin were then amplified and inserted into pENTR/TEV/D-TOPO vector (Invitrogen). The adenovirus was produced using the Invitrogen adenoviral expression system (Invitrogen).

Immunofluorescence assay.

Cardiac myocytes were permeabilized with 0.5% Triton X-100 and blocked with 10% normal goat serum. The sections were incubated with anti-RyR monoclonal antibody (Sigma, R128) for 2 hours at room temperature, washed with PBS and then incubated with tetrarhodamine isothiocyanate (TRITC)-conjugated goat anti-rabbit IgG (Santa Cruz) for 1 hour at room temperature. The immunofluorescence staining was visualized using Zeiss LSM710 confocal microscope at 488nm (GCaMP6f-T/J) and 543 nm (TRITC) excitation and 490-550 and >560nm emission, respectively.

Unmixing of Di-4 AN (F) PPTEA and GCaMP6f-J signals.

Di-4 AN (F) PPTEA (Di-4, 0.5μg/mL, 5 min), a lipophilic dye[19], was used to stain the surface membrane and T-tubules in cultured cardiac myocytes expressing GCaMP6f-J. With excitation at 488nm, spectral images covering 486-719 nm were collected with an inverted confocal microscope (Zeiss NLO710) equipped with a 34-Channel QUASAR Detection Unit. For unmixing the Di-4 and GCaMP6f-J components, the reference spectra were obtained in Di-4-stained, uninfected cells and GCaMP6f-J-expressing, Di-4-unstained cells, respectively.

In situ calibration of the biosensor.

Adult rat cardiac myocytes expressing GCaMP6f-triadin 1/junctin (GCaMP6f-T/J) were permeabilized with 50 μg/ml saponin and then treated with internal solution (IS) containing (in mmol/L) 10 KOH, 100 aspartic acid, 20 KCL, 0.81 $MgCl_2$, 3 Mg-ATP, 0.5 ethylene glycol tetra-acetate (EGTA), 5 phosphocreatine ditris, 10 phosphocreatine-Na, 5 creatine phosphokinase, 10 glutathione, 8% dextran and 20 HEPES and different concentrations of Ca^{2+} (from 3×10^{-9} to 2×10^{-5} mol/L at pH=7.2). The fluorescence of GCaMP6f-T/J was recorded with Zeiss LSM710 confocal microscope with 488 nm excitation and 490-550 nm emission as was also used for fluo-4 measurement. The relationship of Ca^{2+} concentration (C) and normalized fluorescence (R) or $(F-F_{min})/(F_{max}-F_{min})$ where F_{min} and F_{max} were obtained at 3×10^{-9} and 2×10^{-5} mol/L, respectively, was fitted with the equation $R= C^{nH}/(K_d^{nH}+C^{nH})$, where nH is the Hill coefficient and K_d is the dissociation constant.

Confocal imaging.

Confocal imaging was carried out with a Zeiss LSM710 microscope with a 63×, 1.4 N.A. oil immersion objective and linescan speed of 1.53 ms/line, the pinhole was set for a nominal 1μm optical section. For simultaneous measurement of GCaMP6f-T/J and Rhod-2, excitation was at 488 and 543 nm and their fluorescence emission was collected at 490-550 and >560 nm, respectively. For chemical Ca^{2+} indicator loading, cultured cardiac myocytes were incubated with 5 μmol/L rhod-2 AM (Invitrogen) or fluo-4 AM (Invitrogen) for 10 min at room temperature.

Image processing and data analysis.
Digital images were processed using customer-devised routines written in IDL (ITT, New York, NY). To obtain the time course of fluorescence corrected for the biosensor's turn-off kinetics, deconvolution was performed with Wiener filter in the frequency domain. The degenerate kernel used in the Wiener filter was a single-exponential decay function with time constant of 60 ms reflecting the turn-off rate of the biosensor.

Statistics.
Data are reported as the mean ± SE. Student's *t*-test and the Mann-Whitney *U* test for nonparametric distributions were applied, when appropriate, to determine the statistical significance of differences. $P < 0.05$ was considered statistically significant.

RESULTS

Targeting the Ca^{2+} biosensor GCaMP6f to jSR.

The rationale for developing a sensitive (instead of low affinity) targeted Ca^{2+} biosensor is to probe dyad junctional Ca^{2+} dynamics, which has not been possible with cytoplasmic probes. We reasoned that a genetically encoded Ca^{2+} probe linked to known junctional proteins (triadin1 and junctin) should concentrate the biosensor into the high Ca^{2+} nanodomain associated with RyR activity (Fig. 1A). This approach should avoid the potential complication arising from tagging RyRs themselves which might alter their gating and/or assembly in the dyad. As to the biosensor of choice, the latest generation of fluorescent protein-based Ca^{2+} probe GCaMP6f appears to be ideal because of its fast kinetics (the fastest among all currently known GCaMPs), high affinity (relative to junctional calcium), and superb contrast factor[16]. In a very recent study, it was successfully implemented in quantitating single synapse events[16], leading to an important breakthrough in understanding dendritic integration.

In cultured rat ventricular myocytes 48 hours after adenoviral-mediated gene transfer, confocal imaging revealed that GCaMP6f-T or GCaMP6f-J (triadin 1 and junctin constructs respectively) was enriched at punctate sites forming striated sarcomeric pattern (Fig. 1B, C). This result suggests that both triadin 1 and junctin can correctly target their N-terminal fused GCaMP6f to the dyadic clefts. This notion was confirmed by colocalization of GCaMP6f-J and GCaMP6f-T (latter data not shown) with type 2 RyR immunofluorescence (Fig. 1C) and the pattern of labeling was similar to that reported in high resolution studies of RyR distribution[20]. The t-tubular structure of the myocytes was well maintained with GCaMP6f-J and Di-4 fluorescent signals (a surface membrane marker) strongly colocalizing (Fig. 1D) after spectral unmixing (Online Figure I) again supporting the idea that the construct correctly trafficked to the dyadic junctions.

GCaMPs are circularly permuted variants of enhanced green fluorescent protein coupled to the Ca^{2+}-binding protein calmodulin (CaM) at the C terminus as the Ca^{2+} sensor, and a CaM-binding M13 peptide at the N terminus[21]. Crystal structures of GCaMP2 have shown that, upon Ca^{2+} binding, the CaM moiety interacts and interlocks with the M13 peptide, causing a significant structural reorganization in proximity to the chromophore of cpEGFP and increasing its fluorescence, probably by deprotonating the chromophore[22]. To assess the performance of the dyad-targeted GCaMP6f-T/J, we measured fluorescence changes in saponin-permeabilized cells when bathing Ca^{2+} was increased from 3 nmol/L to 20 μmol/L. GCaMP6f-T/J in cardiac dyads displayed a contrast factor of 42.5±11 (n=6 cells) defined as the ratio of maximum (F_{max}) to minimum biosensor fluorescence (F_{min}), similar to that observed *in vitro*[16]. Nonlinear fitting yielded a dissociation constant (K_d) of 632 nmol/L and a Hill coefficient (n) of 1.77(Fig. 1E). Interestingly, GCaMP6f-T/J displayed an off rate ~4-fold faster than that of native GCaMP6f (see below).

Thus, we have succeeded in creating a novel Ca^{2+} biosensor which colocalizes with t-tubules and RyRs at dyadic clefts, offering a new approach to detecting nanodomain Ca^{2+} changes.

Imaging dyadic Ca^{2+} nanosparks with GCaMP6f-T/J.

Spatially discrete, sudden, and transient GCaMP6f-T/J fluorescence increases ("Ca^{2+} nanosparks" –see Discussion) arose spontaneously from biosensor-labeled dyads in resting cardiac myocytes (Fig. 2A, B). Nanosparks rose abruptly, attained a peak of 3.0 (F/F_0) in ~22 ms, and then returned to the baseline with single-exponential kinetics (τ_{decay}~ 63 ms) (Fig 2, Table 1). Individual nanosparks were confined to focal regions of the cell (width ~540 nm, Table 1), with no evidence of a diffusive fluorescence signal affecting ambient space (or neighboring sites). Given the limited confocal resolution, the size of these regions appears consistent with recent tomographic data on dyadic junctions[23]. When compared to Ca^{2+} sparks reported by rhod-2 (Fig. 2C), Ca^{2+} nanosparks occupied a 50-times smaller optical volume but were significantly brighter (Table 1). Ca^{2+} nanosparks were completely abolished by SR-Ca^{2+} depletion with 20 mmol/L caffeine, but persisted in the presence of the LTCC inhibitor nifedipine (10 μmol/L) (data not shown). Hence, these GCaMP6f-T/J fluorescent nanosparks reflect the first direct visualization of Ca^{2+} signals in the dyad junctional space.

The immobility of GCaMP6f-T/J implies that Ca^{2+} nanospark formation is simply driven by the local Ca^{2+} turning ON the biosensor, convolved with the biosensor's OFF kinetics. Specifically, the ON process reflects the rise of local Ca^{2+}, the Ca^{2+} binding to the CaM moiety of the biosensor, and the deprotonating rearrangement around the chromophore prior to fluorescence emission, whereas the OFF process (K_{OFF}) reflects the deactivation of the chromophore. Following RyR closure, local Ca^{2+} gradients collapse rapidly[24, 25] so that the onset of nanospark decline should give a measure of the time taken for complete RyR closure, and the decline rate of nanosparks should be mainly determined by the OFF kinetics of the biosensor. Furthermore, the time course and amplitude (F/F_0) of nanosparks should not depend on relative position of the dyad to the confocal plane, providing that contaminating background fluorescence from other sources is negligible (see below).

As shown in Table 1, the time to peak of nanosparks was longer than the typical time to peak of a Ca^{2+} spark[8]. The histogram of τ_{decay} exhibited a major Gaussian component that centered around 60 ms, with a small tail reflecting a subpopulation of prolonged release events (Online Figure II). These data suggest that the turn-off rate of the targeted biosensor *in situ* was around 17 s^{-1}, a ~4-fold improvement compared to its tag-free counterpart[16]. Importantly, by simultaneously measuring rhod-2 Ca^{2+} signals, we found that the presence of the biosensors did not significantly alter the time course or amplitude of spontaneous Ca^{2+} sparks (Table 1). This result indicates that biosensor expression exerted negligible buffering effects on the evolution of dyadic Ca^{2+} that controls EC coupling.

Based on the nanospark formation mechanism described above, the time course measurement can be improved by temporal deconvolution using a kernel reflecting the turn-off kinetics of the biosensor. Using K_{OFF}= 17 s^{-1} to approximate the OFF kinetics of the biosensor, we deconvolved the nanospark and used the resulting trace, $(F/F_0)_d$, as a more direct indicator of junctional Ca^{2+} dynamics (Fig. 2B). A representative linescan image of kinetically deconvolved Ca^{2+} nanospark $(F/F_0)_d$ and its corresponding spatially averaged line plot are shown in Fig.2B. On average, $(F/F_0)_d$ reached its peak at ~12 ms from onset, in reasonable agreement with detailed modeling and release flux calculations for rat with the release flux reaching a peak at ~5 ms and lasting for ~20 ms[24, 26].

RyR array operation at single dyads.

With the precise colocalization of the biosensor and the Ca^{2+} source, the superior dyad-to-background contrast, and the high sensitivity provided by targeted GCaMP6f-T/J, we investigated RyR

array operation at the single-dyad level. Although Ca^{2+} nanosparks generally appeared as a single homogeneous region, in some cases distinct substructure could be resolved. Fig. 2D illustrates such an event with the fluorescence increase occurring in two linked regions nearly simultaneously (as far as can be determined from the limited time resolution of the microscope and signal to noise ratio). We suggest that such events reflect the activation of separate RyR clusters within the same junctional space which co-activate in <4 ms. Further, we found that the Ca^{2+} nanospark amplitude, measured at the origin of Ca^{2+} release and relatively immune to out-of-focus blurring, displayed a broad distribution (Online Figure IIIA), ranging from 1. 8 to 4.8 (F/F_0 at 5 and 95 percentiles) with a mean value of 3.04. Similarly, after temporal deblurring, peak $(F/F_0)_d$ varied from 4.1 (at 5%) to 14.9 (at 95%) (Online Figure IIIB). Taken together, these data provide novel evidence for the possibility of stochastic recruitment of different numbers of RyRs within Ca^{2+} nanosparks.

We also examined dyads displaying more than one Ca^{2+} nanospark. Fig. 3A&B illustrate variability in peak F/F_0 and $(F/F_0)_d$ in consecutive Ca^{2+} nanosparks. The smallest Ca^{2+} nanosparks similar to single-quanta[13] and "quarky" Ca^{2+} release events reported previously[27]. For pairs of Ca^{2+} nanosparks at the same dyads, their peak F/F_0 ranged from 0.75 to 1.33 (at 5 and 95 percentiles, respectively) with peak $(F/F_0)_d$ from 0.48 to 2.2 (Fig.3C). Thus, the gradation of amplitude reflects an event-to-event stochastic recruitment of individual or sub-clustered RyRs.

Imaging dyadic activation during EC coupling.

Next, we examined junctional Ca^{2+} dynamics during normal (i.e. electrically evoked) EC coupling. Representative results in Fig. 4 illustrate several novel features. First, in cardiac myocytes undergoing electrical pacing, the Ca^{2+} transients occurred in discrete domains that did not merge (unlike other Ca^{2+} reporter signals). Because of this, timing of activation at individual dyads was clearly resolved in vigorously contracting cells. Second, dyads displaying twofold difference in F_0, perhaps reflecting in-focus and slightly out-of-focus sites had similar F/F_0 (Fig. 4B&C). This is due to the probe being fixed so that the relative change in fluorescence is unaffected by the sensitivity of the optical detector (in this case being determined by the limited extent of the microscope point spread function). Third, at dyads that were activated late, we observed a slow transient preceding a sudden, rapid upstroke of the dyadic signal. We interpret the first phase to result from cytosolic Ca^{2+} transient that invades the junctional space, and the second phase to reflect evoked dyadic release in the form of a Ca^{2+} nanospark. Remarkably, the properties of these late Ca^{2+} nanosparks were very similar to those of early ones, directly showing (for the first time) that inferred SR depletion in adjacent sites during EC coupling[28] has minor effects on the proximal SR store on the time scale of normal Ca^{2+} release. Furthermore, the fully activated dyadic Ca^{2+} signal was much higher than the global Ca^{2+} transient alone. The peak $(F/F_0)_d$ in an evoked nanotransient was 7.8-fold higher than that due to global Ca^{2+} elevation, providing direct evidence for a much higher cleft than global Ca^{2+} concentration in EC coupling (as expected from modeling studies).

DISCUSSION

We have developed a novel Ca^{2+} imaging method that has enabled the first detection of Ca^{2+} signals arising in the sub-microscopic (nanoscopic) space of the dyadic junction between the surface membrane and junctional SR. By analogy with Ca^{2+} sparks and to reflect the nanoscopic origin of the signal from our non-diffusible targeted probes we introduce the neologism "Ca^{2+} nanosparks" to describe them. We show that targeted GCaMP6f-T/J provides a new and sensitive way of detecting dyadic activity: i.e. when, where, and for how long a dyad is activated, even in cells undergoing vigorous contraction. Individual Ca^{2+} nanosparks are confined to a volume 50-times smaller than conventional Ca^{2+} sparks as measured with diffusible indicators. Our approach is somewhat analogous to the use of GCaMP6f to

"count" single neuronal synapse events[16]. However, we are dealing with a much smaller structure than a synaptic spine and, in this regard, it is remarkable that our nanoscopic signals had such good fidelity.

Imaging Ca^{2+} nanosparks has been made possible by the availability of a new generation of genetically encoded, ultrasensitive Ca^{2+} biosensor (GCaMP6f) and by the choice of proper targeting strategy. The fast kinetics, the high affinity, the high contrast factor of GCaMP6f collectively confers high sensitivity, while the fusion of biosensor to known dyadic proteins assures precise colocalization to the dyadic Ca^{2+} nanodomain. That the Ca^{2+} biosensor is immobile carries major advantages: Not only does it permit a simple deconvolution to correct for the biosensor's turn-off kinetics, but also it obviates spatial blurring due to out-of-focus sampling that has confounded Ca^{2+} spark measurements. Serendipitously, we also found that the fusion of triadin/junctin to the C terminus of the biosensor also accelerated the turn-off rate of the biosensor, perhaps by facilitating the undocking of the M13-CaM complex. This suggests that further C-terminal modification might present a new strategy to further improve the kinetic properties of GCaMPs.

Whilst being highly sensitive, this new nanodomain Ca^{2+} measurement method also has a wide dynamic range. For example, it allows resolution of "quarky" Ca^{2+} release, spontaneous Ca^{2+} nanosparks and even evoked Ca^{2+} nanosparks during the cell-wide Ca^{2+} transient. Analysis of the variability of Ca^{2+} nanospark amplitude provided new evidence that Ca^{2+} release is not necessarily "all or none" at the level of single dyads. Even at the same dyads, amplitudes of consecutive Ca^{2+} nanospark can vary ~ 2-fold. These results imply stochastic recruitment of different numbers or subclusters of RyRs in a single functional dyadic junction. Our observation of some sub-structure within occasional Ca^{2+} nanosparks further supports the idea of possible subcluster activation within groups of RyRs[29] and previous reports of graded Ca^{2+} spark amplitude [13, 14]. However, we have not yet observed temporally separable Ca^{2+} release events behavior within detectable sub-regions of single junctions, suggesting that RyR subclusters are spatio-temporally (and functionally) coupled within the ~2 ms/0.3 μm resolution of the microscope. From this, we suggest that intra-junctional activation propagation delays should be a minor component of the time to peak of the Ca^{2+} spark, consistent with Monte-Carlo simulations of the effect of RyR (re)organization on release time course within a single junctional region[30].

By tracking individual dyad activation within the whole-cell contraction, the current work represents a substantial improvement over the previous Ca^{2+} spike method using heavy Ca^{2+} buffering[12]. It is especially important to note that the local biosensor did not disrupt normal EC coupling (as evidenced by a lack of effect on Ca^{2+} sparks). Therefore, while there may be some limited junctional buffering effect due to the sensor, cell wide Ca^{2+} signals and Ca^{2+} dependent regulation should be minimally perturbed.

Despite the biosensor's moderate K_d and the high Ca^{2+} concentration expected at the active dyads, we detected no sign of GCaMP6f-T/J saturation during a nanospark: the amplitude of nanosparks is smaller than that of nanotransients during action potential-elicited EC coupling and both were smaller than maximal GCaMP6f-T/J that could be obtained in steady-state calibrations. A possible explanation is that the relatively slow kinetics of the biosensor do not allow the biosensor to equilibrate during the saturating but short-lived dyadic cleft Ca^{2+} transient. Thus, a high-affinity, slowly-responding probe may present relatively low-affinity behavior during highly dynamic Ca^{2+} signals. Furthermore, nonlinear interplay among multiple sensor Ca^{2+}-binding sites and temporal disparity between Ca^{2+}-binding and biosensor fluorescence may also contribute to this peculiar non-equilibrium property of the biosensor. These possibilities warrant future investigation and tuning of biosensor properties but are outside the scope of this article.

As a general problem that applies to all conventional fluorescent Ca^{2+} indicators, Ca^{2+} spark measurement with diffusible indicators grossly underestimates the local peak Ca^{2+} levels and reports a highly distorted spatial profile of local Ca^{2+} gradients[31]. While the targeted sensors GCaMP6f-T/J can

reveal Ca^{2+} release timing in the smallest domains (e.g., a single dyad), we have not yet achieved the ambitious goal of directly reporting local Ca^{2+} levels within the junctional space, for reasons discussed above. Nevertheless, with the highly sensitive biosensor expressed at levels that did not significantly affect junction function, we obtained a Ca^{2+} signal (after temporal deblurring) that should provide an accurate measure of the local Ca^{2+} release duration and semi-quantitative measurement of local Ca^{2+} fluxes.

Since heart failure and cardiac arrhythmias are often associated with dyssynchronous Ca^{2+} release, the ability of the probe to report release timing with good fidelity should facilitate investigation of the synchrony (or dys-synchrony) among release sites in health and diseases[32, 33] . Our targeted Ca^{2+} biosensor approach may be extended to whole tissues and living organisms by transfection or transgenic techniques, and the lack of apparent effect of the biosensor on Ca^{2+} signaling suggests that it should not prevent normal Ca^{2+}-dependent signaling processes (e.g. nuclear and cytoplasmic CaM signaling).

In summary, we have shown that high-quality intra-junctional Ca^{2+} release signals can be recorded as "Ca^{2+} nanosparks" with a novel targeted ultrasensitive biosensor. These Ca^{2+} nanosparks reveal junctional Ca^{2+} signaling in a way that is not possible with conventional diffusible Ca^{2+} indicators. Furthermore, this approach should be generally applicable to probing Ca^{2+} nanodomains (e.g., clusters of IP_3 receptor Ca^{2+} release channels) in many cell types and even in living animals by transfection or transgenic approaches.

ACKNOWLEDGEMENTS

We thank Dr. Looger from HHMI for the generous gift of GCaMP6 vectors and Dr. Leslie M. Loew from University of Connecticut Health Center for Di-4 AN(F)PPTEA.

SOURCES OF FUNDING

This work was supported by the National Key Basic Research Program of China (2011CB809100 and 2013CB531200), the National Science Foundation of China (31221002, 31130067, 31123004, 81370203 and 30900264), and the Royal Society UK.

DISCLOSURES

None.

REFERENCES

1. Franzini-Armstrong C, Protasi F, Ramesh V. Comparative ultrastructure of Ca^{2+} release units in skeletal and cardiac muscle. *Annals of the New York Academy of Sciences*. 1998;853:20-30
2. Grantham CJ, Cannell MB. Ca^{2+} influx during the cardiac action potential in guinea pig ventricular myocytes. *Circulation Research*. 1996;79:194-200
3. Allen DG, Blinks JR. Calcium transients in aequorin-injected frog cardiac muscle. *Nature*. 1978;273:509-513
4. Wier WG. Calcium transients during excitation-contraction coupling in mammalian heart: Aequorin signals of canine purkinje fibers. *Science*. 1980;207:1085-1087
5. Grynkiewicz G, Poenie M, Tsien RY. A new generation of Ca^{2+} indicators with greatly improved fluorescence properties. *The Journal of Biological Chemistry*. 1985;260:3440-3450

6. Cannell MB, Berlin JR, Lederer WJ. Intracellular calcium in cardiac myocytes: Calcium transients measured using fluorescence imaging. *Society of General Physiologists series*. 1987;42:201-214
7. Wier WG, Cannell MB, Berlin JR, Marban E, Lederer WJ. Cellular and subcellular heterogeneity of $[Ca^{2+}]_i$ in single heart cells revealed by fura-2. *Science*. 1987;235:325-328
8. Cheng H, Lederer WJ, Cannell MB. Calcium sparks: Elementary events underlying excitation-contraction coupling in heart muscle. *Science*. 1993;262:740-744
9. Cheng H, Lederer WJ. Calcium sparks. *Physiol Rev*. 2008;88:1491-1545
10. Stern MD. Theory of excitation-contraction coupling in cardiac muscle. *Biophysical journal*. 1992;63:497-517
11. Wang SQ, Wei C, Zhao G, Brochet DX, Shen J, Song LS, Wang W, Yang D, Cheng H. Imaging microdomain Ca^{2+} in muscle cells. *Circulation Research*. 2004;94:1011-1022
12. Song LS, Sham JS, Stern MD, Lakatta EG, Cheng H. Direct measurement of SR release flux by tracking 'Ca^{2+} spikes' in rat cardiac myocytes. *The Journal of Physiology*. 1998;512 (Pt 3):677-691
13. Wang SQ, Song LS, Lakatta EG, Cheng H. Ca^{2+} signalling between single L-type Ca^{2+} channels and ryanodine receptors in heart cells. *Nature*. 2001;410:592-596
14. Wang SQ, Stern MD, Rios E, Cheng H. The quantal nature of Ca^{2+} sparks and *in situ* operation of the ryanodine receptor array in cardiac cells. *Proceedings of the National Academy of Sciences of the United States of America*. 2004;101:3979-3984
15. Cannell MB, Kong CH. Local control in cardiac E-C coupling. *Journal of Molecular and Cellular Cardiology*. 2012;52:298-303
16. Chen TW, Wardill TJ, Sun Y, Pulver SR, Renninger SL, Baohan A, Schreiter ER, Kerr RA, Orger MB, Jayaraman V, Looger LL, Svoboda K, Kim DS. Ultrasensitive fluorescent proteins for imaging neuronal activity. *Nature*. 2013;499:295-300
17. Zhang L, Kelley J, Schmeisser G, Kobayashi YM, Jones LR. Complex formation between junctin, triadin, calsequestrin, and the ryanodine receptor. Proteins of the cardiac junctional sarcoplasmic reticulum membrane. *The Journal of Biological Chemistry*. 1997;272:23389-23397
18. Huang X, Sun L, Ji S, Zhao T, Zhang W, Xu J, Zhang J, Wang Y, Wang X, Franzini-Armstrong C, Zheng M, Cheng H. Kissing and nanotunneling mediate intermitochondrial communication in the heart. *Proceedings of the National Academy of Sciences of the United States of America*. 2013;110:2846-2851
19. Yan P, Acker CD, Zhou WL, Lee P, Bollensdorff C, Negrean A, Lotti J, Sacconi L, Antic SD, Kohl P, Mansvelder HD, Pavone FS, Loew LM. Palette of fluorinated voltage-sensitive hemicyanine dyes. *Proceedings of the National Academy of Sciences of the United States of America*. 2012;109:20443-20448
20. Soeller C, Crossman D, Gilbert R, Cannell MB. Analysis of ryanodine receptor clusters in rat and human cardiac myocytes. *Proceedings of the National Academy of Sciences of the United States of America*. 2007;104:14958-14963
21. Nakai J, Ohkura M, Imoto K. A high signal-to-noise Ca^{2+} probe composed of a single green fluorescent protein. *Nat Biotechnol*. 2001;19:137-141
22. Wang Q, Shui B, Kotlikoff MI, Sondermann H. Structural basis for calcium sensing by GCaMP2. *Structure*. 2008;16:1817-1827
23. Hayashi T, Martone ME, Yu Z, Thor A, Doi M, Holst MJ, Ellisman MH, Hoshijima M. Three-dimensional electron microscopy reveals new details of membrane systems for Ca^{2+} signaling in the heart. *Journal of Cell Science*. 2009;122:1005-1013
24. Laver DR, Kong CH, Imtiaz MS, Cannell MB. Termination of calcium-induced calcium release by induction decay: An emergent property of stochastic channel gating and molecular scale architecture. *Journal of Molecular and Cellular Cardiology*. 2013;54:98-100
25. Soeller C, Cannell MB. Numerical simulation of local calcium movements during L-type calcium channel gating in the cardiac diad. *Biophysical Journal*. 1997;73:97-111

26. Kong CH, Laver DR, Cannell MB. Extraction of sub-microscopic Ca fluxes from blurred and noisy fluorescent indicator images with a detailed model fitting approach. *PLoS Computational Biology*. 2013;9:e1002931
27. Brochet DX, Xie W, Yang D, Cheng H, Lederer WJ. Quarky calcium release in the heart. *Circulation Research*. 2011;108:210-218
28. Picht E, Zima AV, Shannon TR, Duncan AM, Blatter LA, Bers DM. Dynamic calcium movement inside cardiac sarcoplasmic reticulum during release. *Circulation Research*. 2011;108:847-856
29. Baddeley D, Jayasinghe ID, Lam L, Rossberger S, Cannell MB, Soeller C. Optical single-channel resolution imaging of the ryanodine receptor distribution in rat cardiac myocytes. *Proceedings of the National Academy of Sciences of the United States of America*. 2009;106:22275-22280
30. Cannell MB, Kong CH, Imtiaz MS, Laver DR. Control of sarcoplasmic reticulum Ca^{2+} release by stochastic RyR gating within a 3D model of the cardiac dyad and importance of induction decay for cicr termination. *Biophysical journal*. 2013;104:2149-2159
31. Smith GD, Keizer JE, Stern MD, Lederer WJ, Cheng H. A simple numerical model of calcium spark formation and detection in cardiac myocytes. *Biophysical Journal*. 1998;75:15-32
32. Litwin SE, Zhang D, Bridge JH. Dyssynchronous Ca^{2+} sparks in myocytes from infarcted hearts. *Circulation Research*. 2000;87:1040-1047
33. Heinzel FR, MacQuaide N, Biesmans L, Sipido K. Dyssynchrony of Ca^{2+} release from the sarcoplasmic reticulum as subcellular mechanism of cardiac contractile dysfunction. *Journal of Molecular and Cellular Cardiology*. 2011;50:390-400

FIGURE LEGENDS

Figure 1. Targeting the Ca^{2+} biosensor to dyadic clefts. A, Targeting strategies. GCaMP6f was fused to the N-terminus of the dyadic proteins triadin 1 (GCaMP6f-T) or junctin (GCaMP6f-J) and was expressed in cultured adult rat ventricular myocytes by adenoviral infection. **B**, Intracellular localization of GCaMP6f-T. Note the punctate appearance of the fluorescence. **C**, Panels show (from top to bottom) GCaMP6f-J fluorescence, RyR2 immunolabelling and co-localization of GCaMP6f-J and RyR2. Similar results were found with GCaMP6f-T. **D**, Panels show (from top to bottom) GCaMP6f-J fluorescence, the surface membrane marker Di-4 and merged image. Note the preservation of radial t-tubule structure and that the punctate GCaMP6f-J fluorescence occurs along the t-tubules. **E**, *In situ* calibration. Saponin-permeabilized, biosensor-expressing cardiac myocytes were exposed to a solution containing the indicated free Ca^{2+}. F_{min} and F_{max} were measured at 3 nmol/L and 20 μmol/L Ca^{2+}, respectively. The solid curve is a Hill equation fit to the data with parameters as indicated.

Figure 2. Ca^{2+} nanosparks probed with GCaMP6f-T/J. A, Left: Linescan image of a Ca^{2+} nanospark detected with GCaMP6f-T. Right: Time course of fluorescence change and an exponential fit to the rise and the decay (solid line). **B**, Exemplar Ca^{2+} nanospark detected with GCaMP6f-J. Left: linescan image before (top) and after deconvolution using a single-exponential kernel (bottom) reflecting a biosensor's K_{OFF}~17 s^{-1}. Right: original (upper trace, F/F_0) and deconvolved time course (lower trace, $(F/F_0)_d$) of the nanospark. **C,** The top panel shows a typical Ca^{2+} nanospark (left) with a simultaneously recorded Ca^{2+} spark using rhod-2 (right). The bottom panel shows time course and spatial extent of both event signals. Note the slower decay time but decreased spatial extent of the Ca^{2+} nanospark (green) compared to the Ca^{2+} spark (red). **D,** Example of substructure present in some Ca^{2+} nanosparks. The surface plot at the right shows the space-time evolution of the intra-junctional signal.

Figure 3. Ca^{2+} release at single dyads. A, Ca^{2+} nanosparks of variable amplitudes. From top to bottom: raw (top) and normalized (F/F_0) linescan images, time course of the nanosparks and their corresponding deconvolved trace $(F/F_0)_d$. The dashed circle in the F/F_0 image and the arrow in the line plots indicate a quarky Ca^{2+} release event in the decline phase of the first nanospark. **B**, Another example as in A. Note the changing strength of the consecutive Ca^{2+} nanosparks at the same dyad. **C,** Histogram showing single-dyad variability of Ca^{2+} nanospark amplitudes. 109 pairs of nanosparks at the same dyads were obtained and their pair-wise ratios of the nanospark amplitude (F/F_0, blank bars; $(F/F_0)_d$, filled bars) are plotted.

Figure 4. Dyadic Ca^{2+} signals in electrically paced cardiac myocytes. A, Evoked Ca^{2+} nanosparks in a cardiac myocyte under 1Hz pacing. Arrows indicate late release events which can be clearly seen superimposed on the local Ca^{2+} changes. The distortion of the traces was due to cell contraction, showing normal EC coupling was taking place. Solid arrowhead indicates a spontaneous nanospark. **B**, Time course of evoked signals. The time course of F/F_0 for the 2 regions indicated in A, note the synchrony of the fluorescence changes although of differing brightness. This mainly reflects position of the confocal line scan relative to the dyad. **C,** shows that the normalized (to pre-stimulus fluorescence) fluorescence has essentially the same amplitude during the Ca^{2+} transient. Therefore the actual probe fluorescence change is not dependent on position relative to the confocal plane. **D**, Comparison of fluorescence changes during individual transients from a region (red) showing occasional late Ca^{2+} release events: (i and iv) Sudden rise of dyadic Ca^{2+} after a delay. ii: Synchronous activation of the dyad with others across the cell. iii: dyad activation failure. **E**, as in **D**, for $(F/F_0)_d$ on an expanded time scale.

DOI: 10.1161/CIRCRESAHA.114.302938

Table 1. Comparison of Ca^{2+} spark and nanospark properties

Calcium indicator	F/F_0	Time to peak (ms)	T50 (ms)	tau (ms)	FDHM (ms)	FWHM (nm)	n
GCaMP6f-T/J	2.93 ± 0.13	22.5 ± 1.38	36.3 ± 1.97	65.0 ± 3.00	53.2 ± 2.30	542 ± 15.9	48
GCaMP6f-T/J(rhod-2)	3.18 ± 0.17	21.5 ± 1.29	37.9 ± 1.71	61.7 ± 2.78	53.7 ± 2.17	547 ± 17.0	41
rhod-2(GCaMP6f-T/J)	1.77 ± 0.11	21.3 ± 1.55	33.5 ± 4.49	—	49.7 ± 4.80	2196 ± 129	19
rhod-2	1.58 ± 0.05	21.1± 1.77	33.6 ± 2.18	—	48.8 ± 2.49	2068 ± 94.4	37
fluo-4	2.03 ± 0.09	16.1 ± 0.87	30.7 ± 2.58	—	42.2 ± 2.90	2197 ± 93.0	52

Data are presented as mean±s.e.m.. No significant differences between rhod-2 sparks in biosensor-free versus GCaMP6f-T/J expressing cells.

Novelty and Significance

What Is Known?

- In cardiac dyads, junctional Ca^{2+} directly controls the gating of the ryanodine receptors (RyRs) and is itself dominated by RyR-mediated Ca^{2+} release from the sarcoplasmic reticulum.
- The stochastic timing of individual dyad Ca^{2+} release events that produce Ca^{2+} sparks governs the rising phase of the whole cell Ca^{2+} transient.
- Conventional diffusible fluorescent Ca^{2+} indicators are unable to report Ca^{2+} in the dyadic junction, making it impossible to resolve individual dyad events during a fully-activated Ca^{2+} transient.

What New Information Does This Article Contribute?

- A targeted, non-diffusible Ca^{2+} probe was developed by fusing the Ca^{2+} sensor GCaMP6f to the N-terminus of triadin 1 and junctin, GCaMP6f-T/J, which resulted in its colocalization with RyRs.
- GCaMP6f-T/J reported Ca^{2+} nanosparks, which are Ca^{2+} signals associated with dyadic activation. Ca^{2+} nanosparks were spatially 50-times smaller (by volume) than conventional Ca^{2+} sparks.
- Ca^{2+} nanosparks report when, where, and for how long an individual dyad is activated, even during the whole cell Ca^{2+} transient, and can reveal co-activation of subclusters of RyRs in the junction.

Ca^{2+} signaling is the result of nanoscopic Ca^{2+} kinetics in, for example, synapses and cardiac dyads. Imaging with diffusible Ca^{2+} indicators has so far visualized microscopic events such as Ca^{2+} sparks and Ca^{2+} puffs, which reflect the diffusion of Ca^{2+} from the sources, but does not resolve the underlying nanoscopic Ca^{2+} kinetics. By fusing GCaMP6f (a new fast calmodulin-based fluorescent protein) to the N-terminus of triadin 1 or junctin, which are known to traffic to dyads, we developed a non-diffusible Ca^{2+} probe, GCaMP6f-T/J. This probe colocalizes with RyRs and displays 4-times faster off-kinetics than native GCaMP6f. This approach allowed the first detection of "Ca^{2+} nanosparks" at individual dyads, which are 50-times smaller (by volume) than conventional Ca^{2+} sparks. Ca^{2+} nanosparks report when, where, and for how long a dyad is activated, even in cells undergoing vigorous contraction. In addition, we showed co-activation of sub-clusters of RyRs as well as "all-or-none" behavior in a single junctional region. This imaging strategy should be generally applicable to probing Ca^{2+} nanodomains in many cell types and even in living animals by transfection or transgenic approaches.

DOI: 10.1161/CIRCRESAHA.114.302938

Figure 1

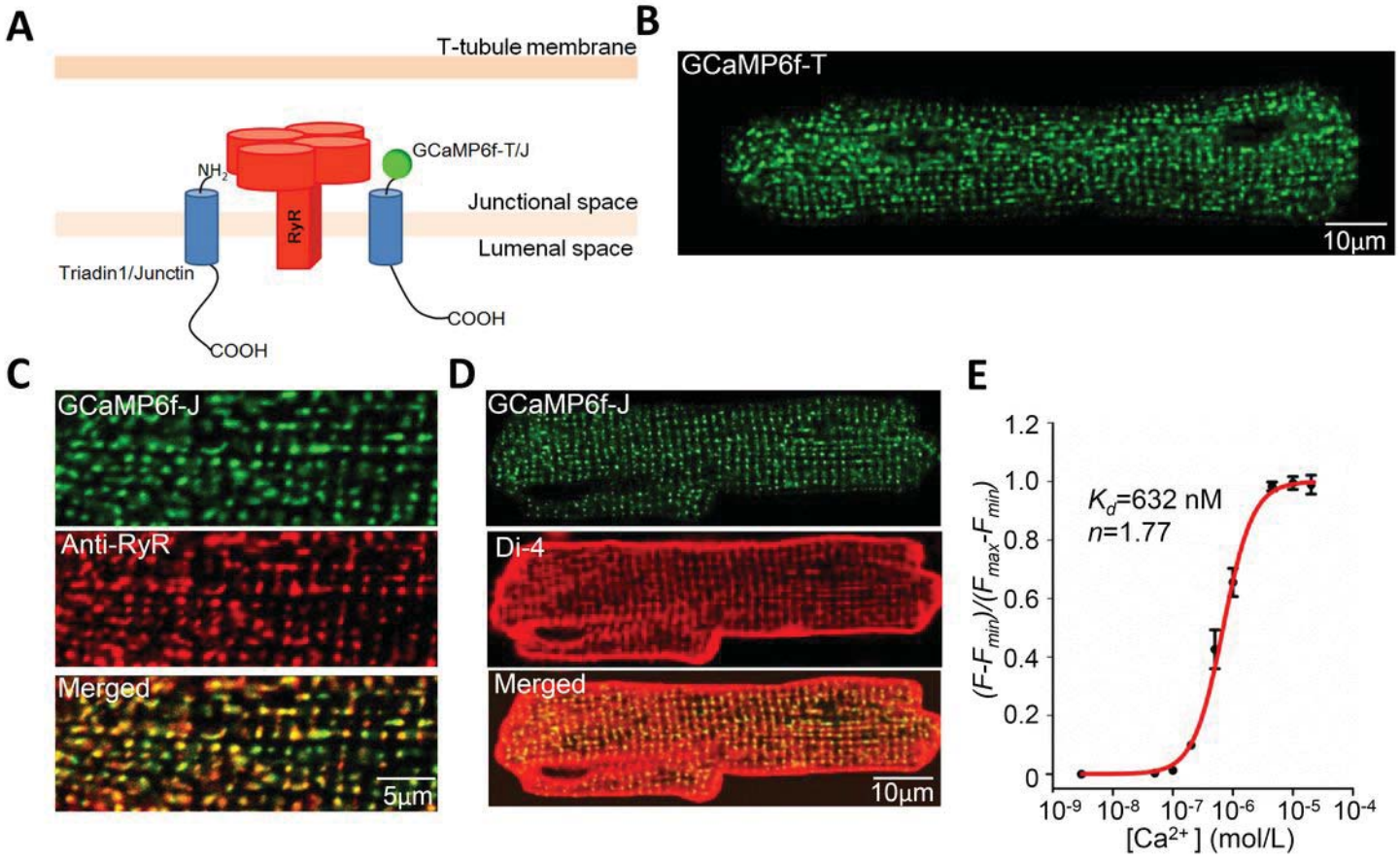

Figure 2

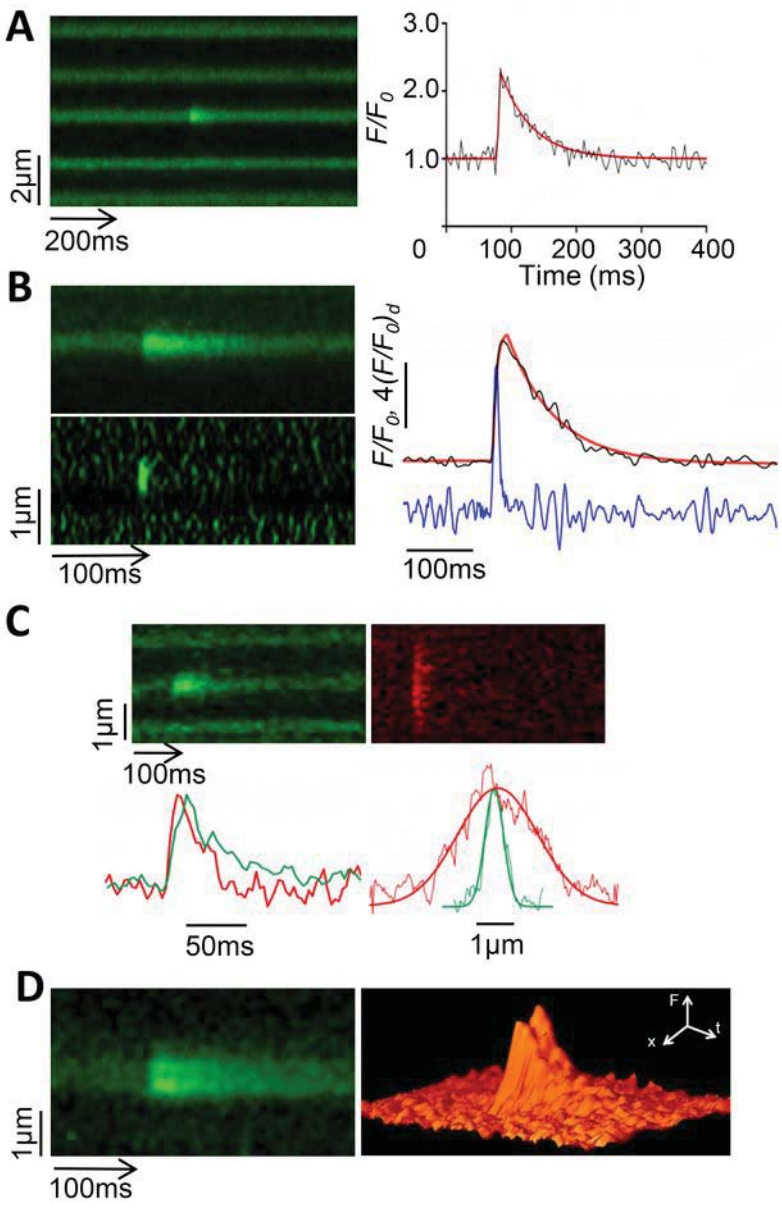

Figure 3

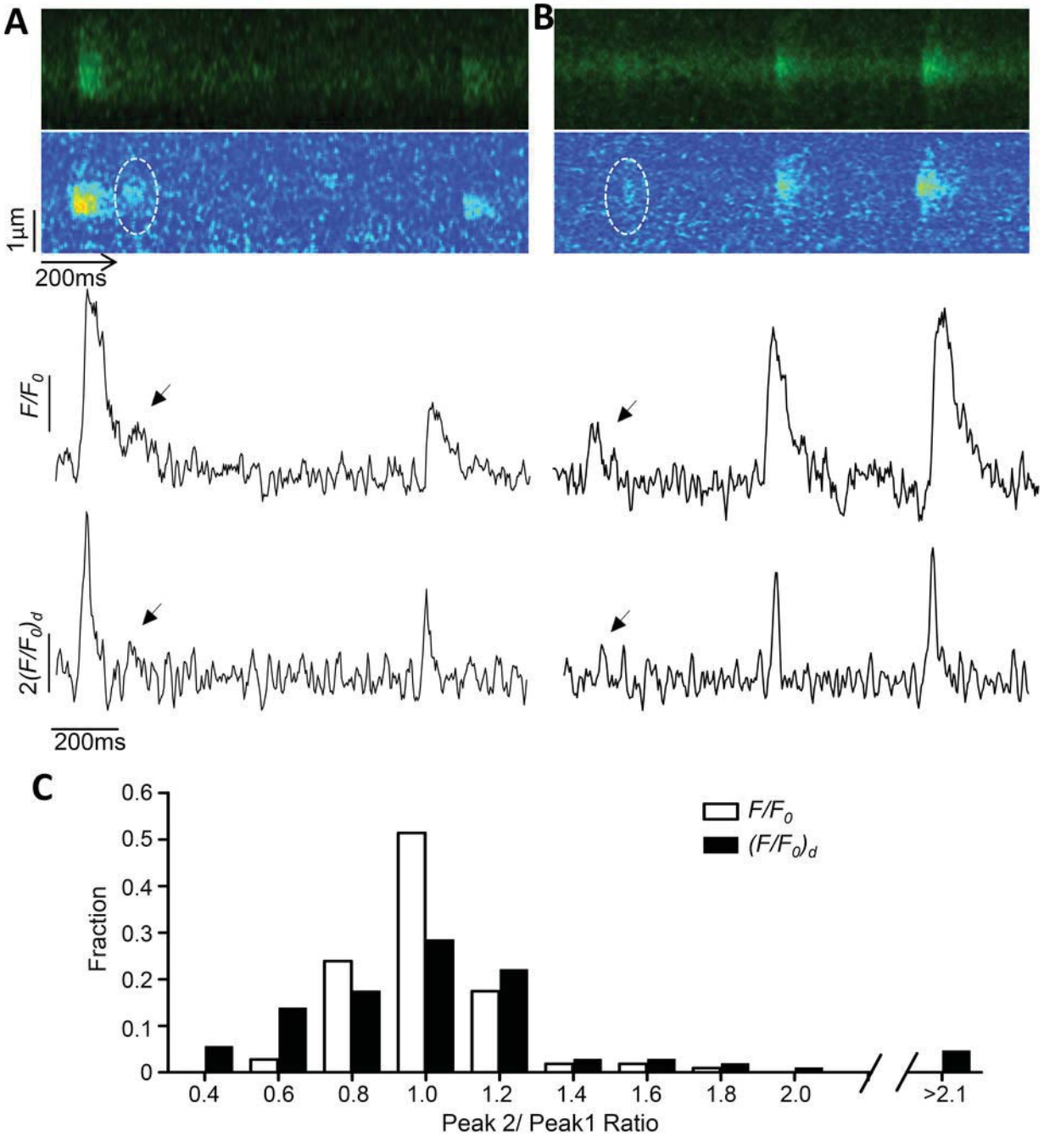

Figure 4

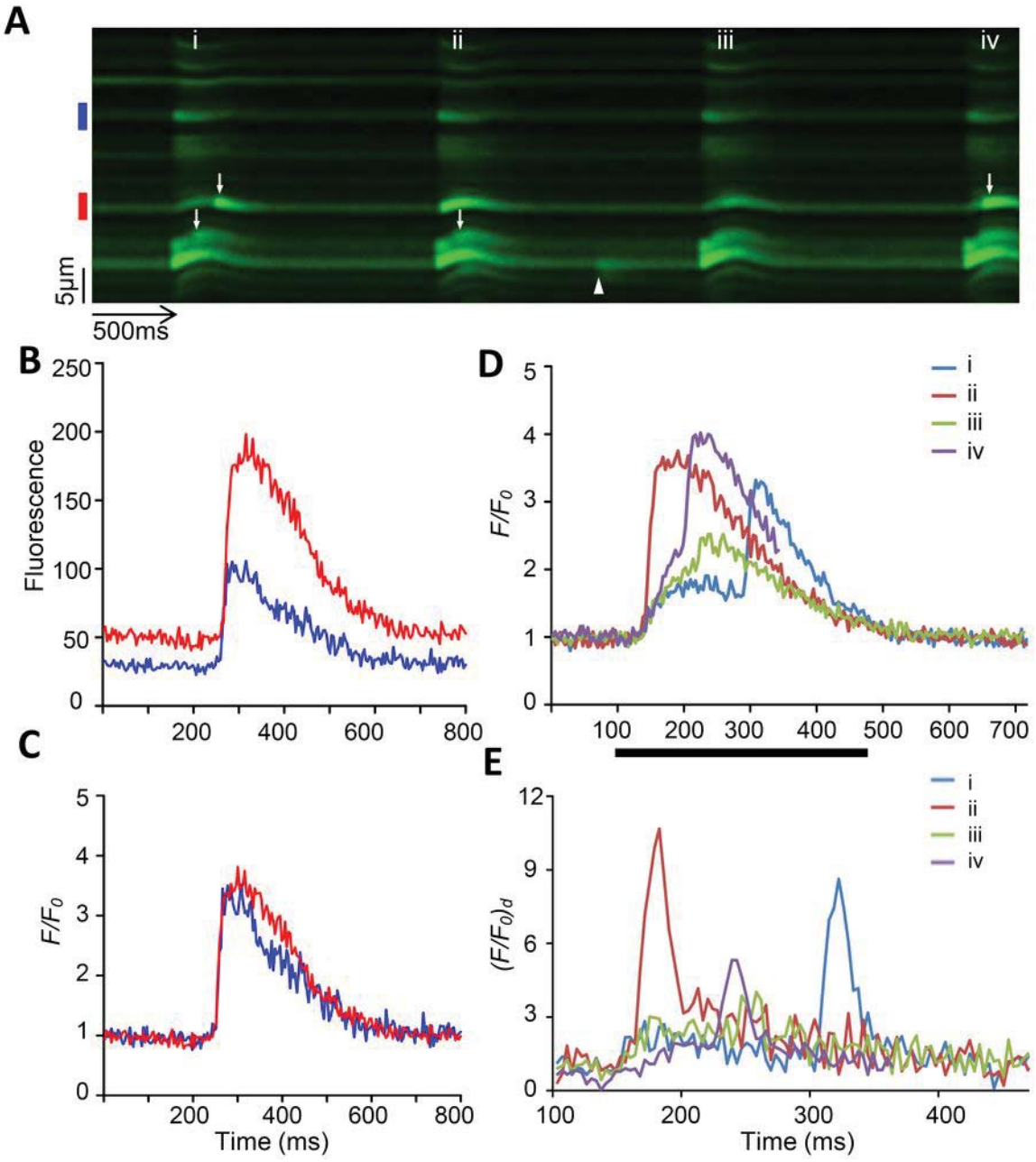

Supplemental Materials

Online Figure I

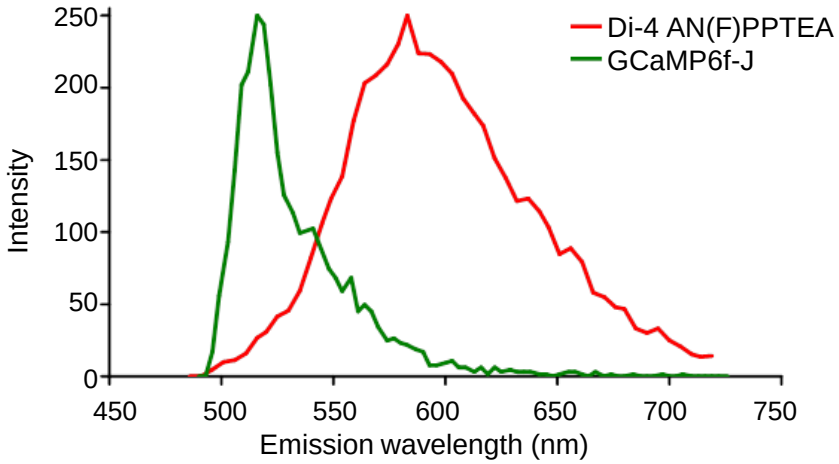

Online Figure I. Spectra of GCaMP6f-J and Di-4 measured in intact cardiac myocytes. These spectra were used for unmixing the data shown in Fig1.**D** to improve spectral separation.

Online Figure II

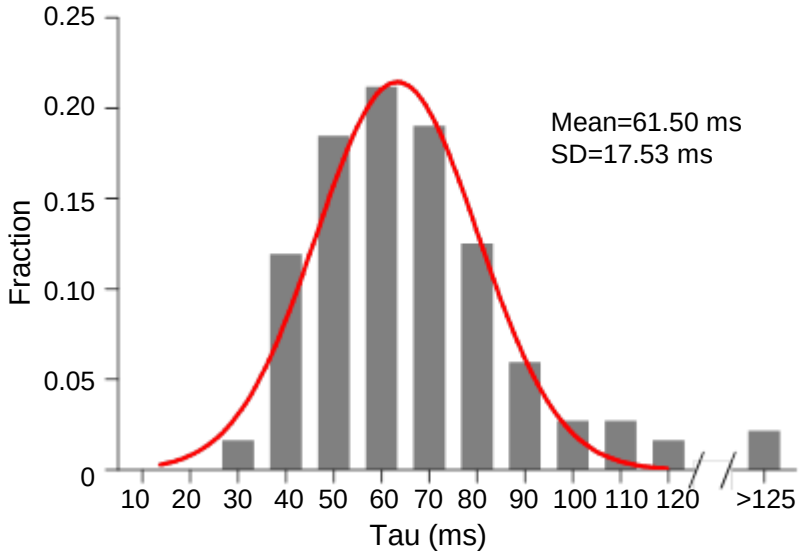

Online Figure II. Histogram of the decay rate constant of nanosparks.
N= 184 events. Solid smooth line represents a Gaussian fit to the data.

Online Figure III

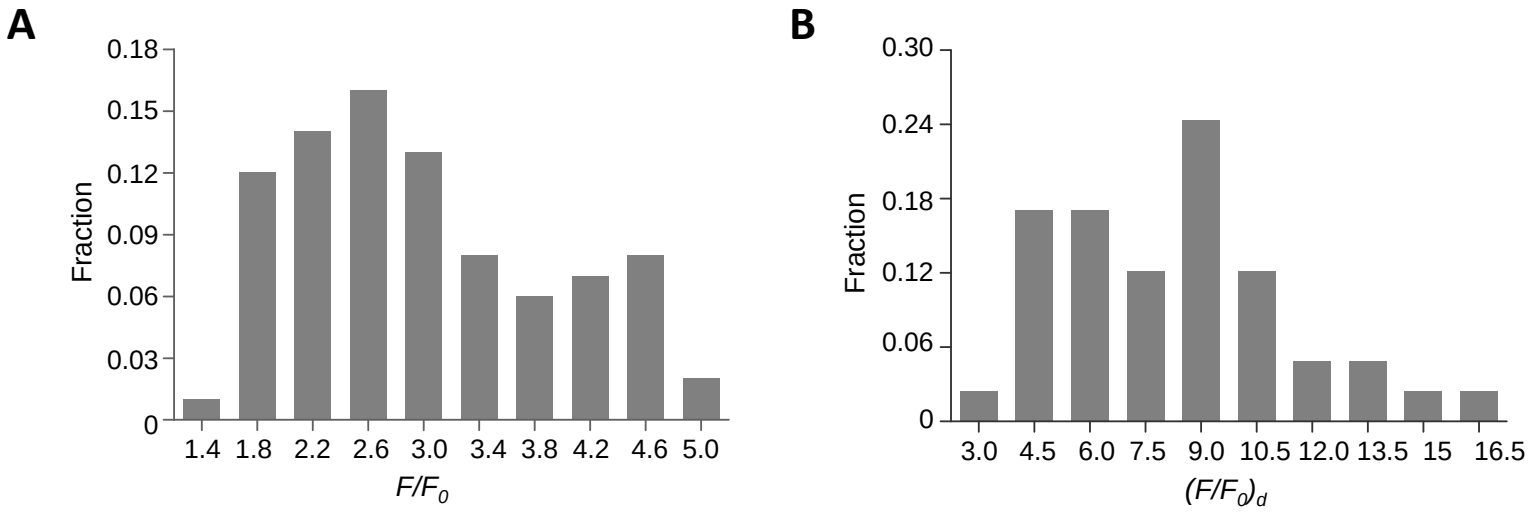

Online Figure III. Histograms for nanospark amplitude measured as peak F/F_0 (A) and peak $(F/F_0)_d$ (B). N= 89 events.